Decoupled Photovoltaic Power Ramp-rate Calculation Method for Perturb and Observe Algorithms

Jose Miguel Riquelme-Dominguez, *Student Member*, *IEEE*, Francisco M. Gonzalez-Longatt, *Senior Member*, *IEEE*, and Sergio Martinez, *Senior Member*, *IEEE*

***Abstract*—As photovoltaic energy increasingly penetrates in power systems, transmission system operators have started to request its participation in providing ancillary services. One of the demanded services is the power ramp-rate control (PRRC), which attempts to limit the power ramps produced by intermittent irradiance conditions. In order to achieve the desired objective, solutions based on storage systems or modifying the maximum power point tracking (MPPT) in perturb and observe (P&O) algorithms are commonly adopted. The starting point in PRRC is the determination of the instantaneous power ramp-rate, and different methods have been proposed in the literature for its calculation. However, the accuracy and computational speed of existing procedures can be improved, which may be critical in situations with rapid irradiance fluctuations. In this paper, a decoupled photovoltaic power ramp-rate calculation method is presented, in which the effect of variable irradiance and the P&O algorithm are computed separately. The proposed method has been theoretically demonstrated and tested through simulation and experimental tests. Simulation results show that it can improve the previous methods in terms of accuracy and computation time. Experimental validation with hardware-in-the-loop demonstrates the suitability of the proposed method for real-time applications, even in presence of noisy measurements.**

***Index Terms*—Hardware-in-the-loop, maximum power point tracking, perturb and observe, photovoltaic, power ramp-rate control, ramp-rate calculation method.**

I. Introduction

SOLAR photovoltaic (PV) is one of the most promising primary energy sources in the future [1]. As the installed capacity is expected to continue to increase, transmission system operators (TSOs) will face new challenges in terms of stability and reliability of modern power systems [2]. One of these challenges is related to the fact that compared with conventional generation, PV systems are sometimes exposed to rapid fluctuations on the primary energy source, i.e., incident solar irradiance, which may cause voltage rise, frequency deviations, and output power fluctuations [3].

A cost-effective manner to reduce the impact of fast irradiance variations is through PV power ramp-rate control (PRRC) [4]. Therefore, on the basis of National Renewable Energy Laboratory (NREL) recommendations [5], different countries have applied limits to output power ramp-rate in the PV generation: the Puerto Rico Electric Power Authority (PREPA) established the ramp-rate limitation of 10%/min of the rated capacity; EirGrid, the Irish TSO, set an absolute limit up to 30 MW/min; the Hawaiian Electric Company (HECO) limited not only the ramp-rate in a minute but also the ramp-rate in shorter periods (2 s). Figure 1 depicts the example of four power ramp-rate limitations when the available power is highly fluctuating.

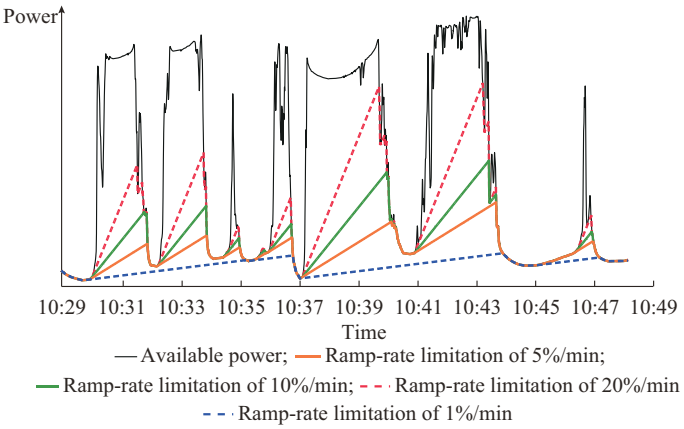

Fig. 1. Example of four different power ramp-rate limitations when available power is higly fluctuating.

In order not to exceed these limits, PRRC must be applied. The development of smart inverters (SIs), which are already required in places such as Hawaii [6], has partially solved the problem of its implementation. However, the DC-AC converter just controls the power injected into the power system; in the case where no energy storage or additional

Manuscript received: September 2, 2021; revised: November 3, 2021; accepted: January 7, 2022. Date of CrossCheck: January 7, 2022. Date of online publication: February 4, 2022.

This work was supported by the Spanish National Research Agency Agencia Estatal de Investigacion (No. PID2019-108966RB-I00/AEI/10.13039/50110001-1033).

J. M. Riquelme-Dominguez (corresponding author) and S. Martinez are with the Electrical Engineering Department, Escuela Tecnica Superior de Ingenieros Industriales, Universidad Politecnica de Madrid, 28006 Madrid, Spain (e-mail: jm.riquelme@upm.es; sergio.martinez@upm.es).

F. M. Gonzalez-Longatt is with the Department of Electrical Engineering, Information Technology and Cybernetics, University of South-Eastern Norway, 3918 Porsgrunn, Norway (e-mail: fglongatt@fglongatt.org).

DOI: 10.35833/MPCE.2021.000603

measuring equipment on the primary energy source is used, the timeliness of the information of possible rapid changes in the incident irradiance can be improved. Furthermore, SIs without stored energy (i. e., without some kinds of storage systems such as batteries) or reserved energy (if the PV system was previously at a curtailed operating point) cannot typically control downward power ramp-rates [7] associated with the rapid decreases of irradiance, if the values of these ramp-rates are greater than the limits specified by the TSO. Thus, the next generation of inverters will need to incorporate new functionalities. In this respect, several methods have been recently proposed in the literature to improve the PV generation capabilities in terms of PRRC. Reference [8] installs ground-based sensors for predictive control of passing clouds. This method provides a high average accuracy, but it requires additional equipment and more complex communication systems. A different method consists in the incorporation of battery energy storage systems (BESSs) [9], [10] that allow to limit not only the ramp-up events but also the ramp-down ones. By using this method, the PV system can operate in the maximum power point tracking (MPPT) mode at any moment, and, when the generated power ramp-rate is larger than the specified limit, the excess of power is used for charging the BESS. Then, the energy available at the BESS can compensate for power generation drops. The main drawbacks of PV systems based on BESS are the cost of the batteries and their reduced lifetime compared with the rest of the system [11], [12].

To overcome the issues exposed above, recent studies have investigated cost-effective implementations of PRRC without energy storage or additional equipment by just modifying the MPPT algorithm. In the most advanced one [13], the operation mode is alternated between the MPPT mode (to extract the maximum power available) and the PRRC mode, in which the operation point is continuously perturbed to the left side of the maximum power point (MPP) when the calculated ramp-rate is larger than the limit. However, two important considerations must be taken into account in this strategy. As the selected MPPT algorithm is the conventional perturb and observe (P&O) [14] algorithm, MPPT drift can occur under variable irradiance conditions [15]. Moreover, the power ramp-rate calculation, determined as the quotient between the power variation and the time variation, ignores the dependence on the P&O perturbation size. In [16], a novel power ramp-rate measurement technique is introduced. This calculation method adjusts the power variation ΔP rather than the time variation Δt in order to avoid any delay. However, its demonstration does not consider the typical waveforms of P&O algorithms.

As reviewed, the trends in PV PRRC precise somehow the real-time (RT) value of the power ramp-rate, which can be either calculated or measured. To improve the above-mentioned power ramp-rate calculation methods, a novel procedure is presented in this paper. The optimized MPPT for fast-changing environmental conditions (dP-P&O) [17] is chosen as the MPPT algorithm. The incorporation of dP-P&O algorithm provides two benefits: the dP-P&O algorithm is able to avoid the MPPT drift, and introduces an additional measurement of power, which gives valuable information in the power ramp-rate calculation process. This information is used by the proposed method to decouple the power ramp-rate caused by the MPPT algorithm and the one caused by irradiance change. Consequently, a noiseless measurement of the RT power ramp-rate can be obtained without any delay, even in highly-variable irradiance scenarios, as demonstrated in the simulation results.

This paper is organized as follows. Section II explains the differences between the conventional P&O and the dP-P&O algorithms. Section III presents the proposed decoupled power ramp-rate calculation method. Section IV shows the simulation results. Section V presents the experimental validation. Finally, Section VI draws conclusions of this paper.

II. Conventional P&O and dP-P&O Algorithms

PV systems are traditionally equipped with MPPT algorithms in order to follow the MPP at every moment. There is a wide range of MPPT algorithms that perform the search of MPP in various ways [18]-[20], optimizing aspects such as the tracking speed, the oscillation in steady-state, or the implementation complexity.

One of the widely used MPPT algorithms is the conventional P&O algorithm, mainly due to the ease of its implementation. The operating principle that governs the P&O algorithm is as follows. While the PV system operates at a specific operating point, defined by its voltage-current coordinates (V_{pv}, I_{pv}), a disturbance in voltage V_{step} is applied, and the variation in power ΔP_{pv} of the system is observed. If the power variation is positive, in the next step, another perturbation will be applied in the same direction as the previous one. Otherwise, the disturbance will be applied in the opposite direction. The flowchart of conventional P&O algorithm is depicted in Fig. 2, where T_M is the perturbation period of the MPPT algorithm.

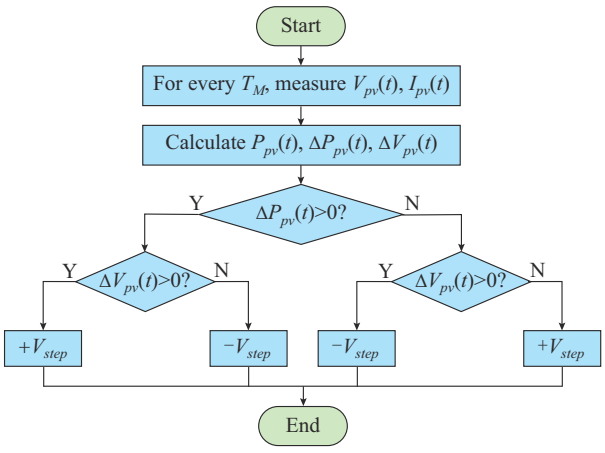

Fig. 2. Flowchart of conventional P&O algorithm.

As can be deduced from the operation of the conventional P&O algorithm, under stable conditions of irradiance and temperature, the operation point oscillates around the MPP. This is known as the three-level operation, and is represented in Fig. 3(b), where points ①-③ are the three-level operating points defined by their coordinates (V_i, P_i), $i = 1, 2, 3$.

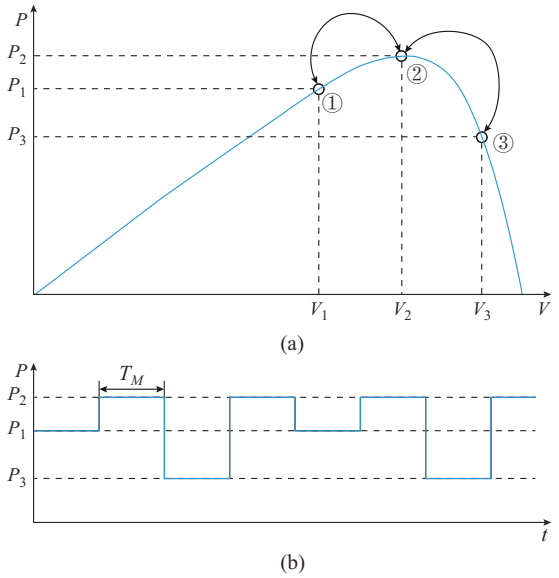

Fig. 3. Principle of operation of conventional P&O algorithm. (a) Conventional P&O algorithm oscillating around MPP. (b) Three-level operation of conventional P&O algorithm.

The main drawback of the conventional P&O algorithm is precisely the oscillation produced around the MPP, which depends directly on the magnitude of the perturbation applied. In addition, under variable irradiance conditions, the conventional P&O algorithm can make wrong decisions because it is not able to identify if the power variation is caused by the perturbation applied or it is due to a change in the incident irradiance. This undesired phenomenon is known as the MPPT drift. To avoid this, some modified P&O algorithms have been presented in the literature. Among them, dP-P&O algorithm [17] shows the best performance under variable irradiance conditions [21]. The novelty of the dP-P&O algorithm compared with the conventional P&O algorithm is introduced in the calculation of ΔP_{pv}, denoted as dP. The calculation procedure can be observed in Fig. 4.

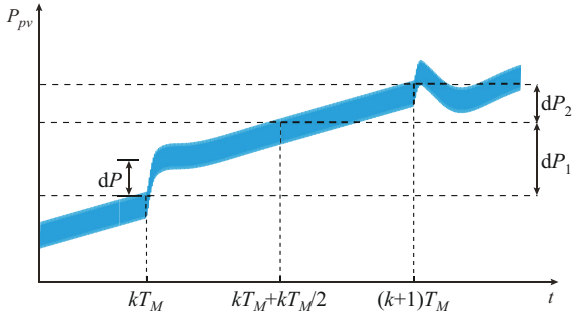

Fig. 4. Calculation procedure of dP-P&O algorithm.

This algorithm assumes that the change in irradiance during an MPPT cycle is constant. In this way, in the first semi-period of the MPPT, the change in power dP_1 is determined by the change in irradiance plus the perturbation of the MPPT algorithm. In the second semi-period, the change in power dP_2 is determined by the change in irradiance only. Finally, the variation in power only due to the MPPT algorithm can be computed as:

$$\mathrm{d}P = \mathrm{d}P_1 - \mathrm{d}P_2 \tag{1}$$

As evidenced, the dP-P&O algorithm decouples the effects of the MPPT algorithm and the variable irradiance. This information can be used not only for MPPT drift avoidance, but also for the determination of the RT power ramp-rate as presented in the following section.

III. Proposed Decoupled Power Ramp-rate Calculation Methods

Power ramps represent the change in power of a system per unit of time. As these ramps can significantly affect the proper functioning of power system, TSOs have started to take measures to limit the ramps that occur in both conventional and renewable generations. In fact, renewable generation is more prone to this type of change due to its volatility and unpredictability [22]. A previous step to PRRC is the calculation of the power ramp-rate in RT. Different methods for power ramp-rate calculation have been proposed in the literature. One of them uses the moving average techniques [23]. This method satisfactorily filters out the oscillations caused by the MPPT algorithm, but introduces significant delays in the calculation, which can affect the performance of the PRRC. A simpler and more direct calculation method is proposed in [13] to reduce this delay. In this method, the ramp-rate calculation is performed with a lower frequency than the execution frequency of the MPPT. Specifically, the ramp-rate $r(t)$ is computed as the difference between two consecutive power measurements divided by the time variation as:

$$r(t) = \frac{P(t) - P(t - nT_M)}{nT_M} \tag{2}$$

where n is the filtering parameter. As can be implicitly deduced from (2), the calculation procedure is not only affected by n, but also by V_{step}. This will be further explained in the following subsections.

A. Dependence on Filtering Value

Reference [13] concludes that a high value of n filters out the inner MPPT oscillations. It is also stated that a higher value of n can introduce significant delays in the ramp-rate calculation. To clarify this influence, Fig. 5 shows the influence of filtering parameter n in power ramp-rate measurement. It depicts a typical P&O power waveform (blue line) in steady state (i.e., when the power ramp-rate caused by irradiance change is zero) and a possible power ramp-rate measurement (red line) depending on n. As mentioned above, depending on the selection of n, different values of the power ramp-rate can be obtained. Particularly, the cases of $n=1$ and $n=5$ could be compared, which have the same power variation. As can be deduced, when considering identical power variation, a greater filtering parameter reduces the influence of the MPPT perturbation. However, a delay proportional to n is introduced. Another interesting case to be considered could be the one with $n=4$, in which the influence of the MPPT perturbation is completely avoided and

the power ramp-rate calculation is computed properly, with a delay of just $3T_M$. Nonetheless, it is important to emphasize that Fig. 5 represents constant irradiance conditions, and when environmental conditions vary, it is impossible to determine beforehand the optimum value of n from the point of view of accuracy in the power ramp-rate calculation.

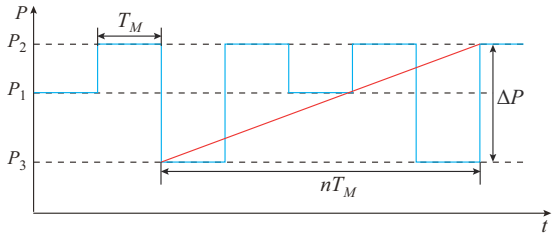

Fig. 5. Influence of filtering parameter n in power ramp-rate measurement.

B. Dependence on Perturbation Size

Implicitly, the power ramp-rate calculation is also affected by the perturbation size V_{step} of the conventional P&O algorithm, as it influences the power variation. Figure 6 illustrates the influence of the perturbation size V_{step} in power ramp-rate measurement. Two P&O power waveforms (the original and the one with reduced Vstep, represented by their three power levels P_1-P_3 and P'_1-P'_3, respectively) in steady-state irradiance conditions differ in the magnitude of the perturbation applied. As can be observed, for the same value of n, a reduced V_{step} gives a lower ramp-rate result, thus providing a more accurate measurement of the change in the incident irradiance. This conclusion, obtained for constant irradiance conditions, can be extrapolated to variable irradiance conditions.

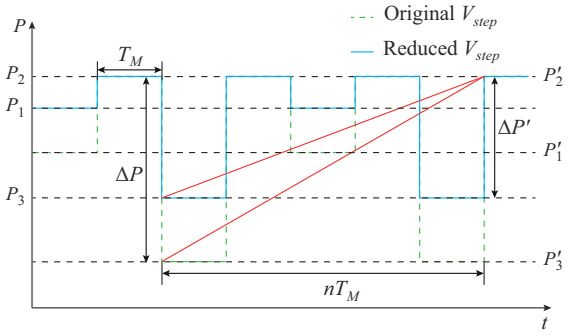

Fig. 6. Influence of perturbation size V_{step} in power ramp-rate measurement.

The main conclusion that can be drawn from the above analysis is that, in order to reduce the error of the calculated power ramp-rate in steady-state, the value of the filtering parameter n should be maximized, and the value of the perturbation size V_{step} should be minimized. However, this combination produces an MPPT algorithm with slow tracking speed due to the small V_{step} parameter and a slow PRRC algorithm due to the introduced delays in the calculation. To overcome these issues, a novel power ramp-rate calculation method based on the dP-P&O algorithm is presented in the following subsection.

C. Proposed Ramp-rate Calculation Method

Previous methods for PV PRRC without energy storage [13], [16] have proposed to modify the MPPT algorithm to achieve the desired objective. In both cases, the chosen MPPT algorithm is the conventional P&O, which suffers from MPPT drift under highly fluctuating irradiance conditions. To solve this problem, the proposed method is based on the dP-P&O algorithm [17], so the MPPT drift situation is completely avoided. Additionally, the dP-P&O algorithm introduces a supplementary power measurement that has been used in the proposed power ramp-rate calculation. This additional power measurement allows the decoupling on the determination of the power ramp-rate caused by the MPPT algorithm and the one caused by the irradiance change. This method is simple and straightforward, and therefore, gives a solution for RT implementation, which makes it suitable for the determination of fast irradiance variations.

The initial hypotheses for the application of the proposed method are twofold: the irradiance change is constant during the MPPT period T_M and the PV system reaches the voltage reference in the first semi-period of the MPPT. Although the latter implies a reduction of the MPPT tracking performance and some delay in the power ramp-rate calculation, they are compensated by the fact that the proposed strategy can minimize the filtering value. Under these conditions, it is possible to decouple the power ramp-rate produced by the irradiance change and the power ramp-rate caused by the MPPT algorithm. Retrieving the nomenclature of Fig. 4, the power ramp-rate expressions can be determined by:

$$r_{irr}(t) = \frac{2\mathrm{d}P_2}{T_M} \tag{3}$$

$$r_{MPPT}(t) = \frac{\mathrm{d}P_1 - \mathrm{d}P_2}{T_M} \tag{4}$$

where $r_{irr}(t)$ and $r_{MPPT}(t)$ are the power ramp-rate produced by the irradiance change and the power ramp-rate caused by the MPPT algorithm, respectively.

As the main contribution of this paper is the use of the dP-P&O algorithm for the power ramp-rate calculation, Fig. 7 shows how this algorithm can be integrated into a PRRC strategy. After voltages and currents are measured, power variations, voltage variations, and power ramp-rates caused by the irradiance change and the perturbation of the MPPT algorithm are calculated. Then, the algorithm considers the operation mode to calculate the total ramp-rate $RR(t)$. This is necessary for neglecting the power ramp-rate introduced by the MPPT when it is active. Finally, the algorithm checks if the ramp-rate is larger than the limit: if so, the voltage perturbation is applied (over the previous reference voltage $V_{ref,prev}$) consecutively to the left of the MPP until the ramp-rate is lower than the limit; otherwise, the MPPT algorithm continues to be enabled.

In order to clarify the advantages of the proposed method, Fig. 8(a) shows the generated PV power of the dP-P&O algorithm when an irradiance ramp profile and two values of the perturbation size V_{step} are considered.

Figure 8(b) and (c) depicts the calculated power ramp-

rates due to the MPPT algorithm and the irradiance change, respectively. As illustrated, the case with a larger value of V_{step} suffers higher power ramp-rate oscillations due to the MPPT algorithm, which is logical. However, both cases obtain a similar value for the power ramp-rate caused by the irradiance change. This result manifests that it is possible to increase the magnitude of the perturbation applied without affecting the PV power ramp-rate calculation.

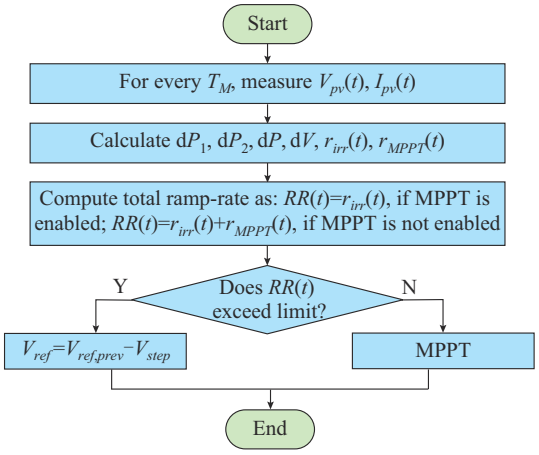

Fig. 7. Integration of proposed power ramp-rate calculation method in a PRRC strategy.

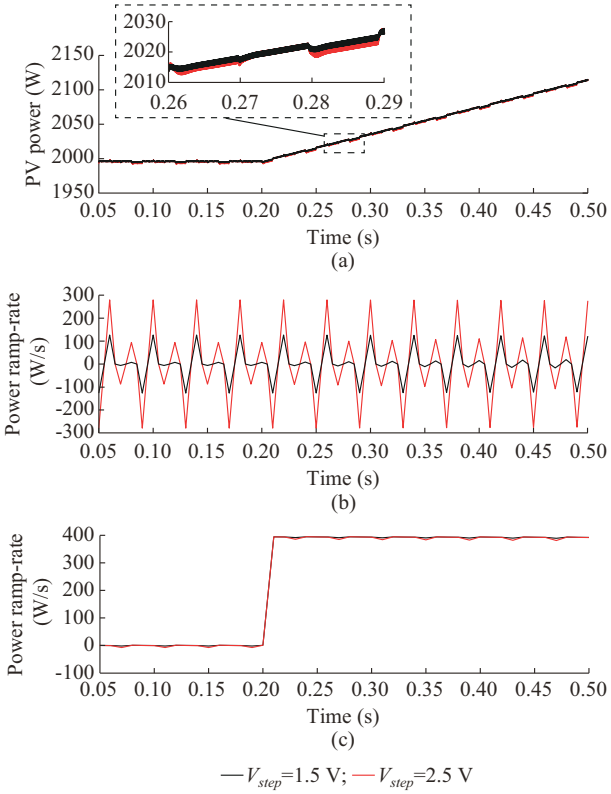

Fig. 8. Evaluation of proposed method with different values of V_{step} applied. (a) Generated PV power. (b) Calculated power ramp-rate due to perturbation of MPPT algorithm. (c) Calculated power ramp-rate due to irradiance change.

Decoupling the power ramp-rate induced by the irradiance change and by the perturbation of MPPT algorithm provides valuable information that may be used in PRRC. In fact, with the proposed method, it is possible to minimize the filtering value, i. e., $n=1$, while maintaining high values of V_{step}, which allows a fast PRRC performance with improved accuracy, as demonstrated in the following simulation results.

IV. Simulation Results (Case Study 1)

The proposed power ramp-rate calculation method has been tested in MATLAB/Simulink [24]. The PV system, control system, and ramp-rate measurement implementation are depicted in Fig. 9.

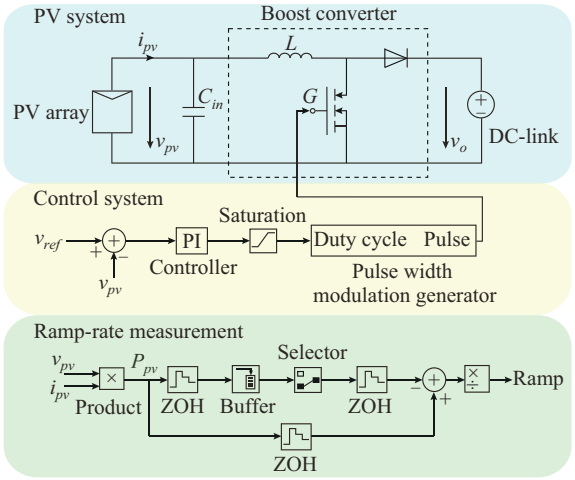

Fig. 9. PV system, control system, and ramp-rate measurement implementation.

As shown in Fig. 9, the PV system is formed by a 2 kW PV array, an input capacitor (C_{in}), a boost converter formed by an inductance (L), a diode, and a transistor whose gate is denoted by G, and the DC-link. The DC-DC converter is controlled by the voltage reference V_{ref}, which is generated by the dP-P&O algorithm, in order to extract the maximum available power. The ramp-rate measurement subsystem is formed by zero-order hold (ZOH) blocks, a buffer, and a selector, and it calculates the power ramp-rate caused by irradiance as discussed in Section III-C. Table I shows the main parameters of the PV system.

TABLE I
Main Parameters of PV System

Parameter	Value
Rated power (P_{MPP})	2000 W
Input capacitance (C_{in})	3.125 μF
Converter inductance (L)	36.6 mH
DC-link voltage (V_o)	350 V
Switching frequency (F_s)	20 kHz

In order to evaluate the adequacy of the proposed method, two case studies are presented for the comparison of the proposed method with the one presented in [13]. Both methodologies have been implemented in the PV system of Fig. 9 with the main parameters collected in Table I.

The first scenario analyzes the effect of varying the filtering parameter n and the perturbation size V_{step} in the power ramp-rate calculation. First of all, the method in [13] is implemented with the following details: the filtering parameter n is maintained equal to the unit while the perturbation size V_{step} takes different values, namely 1, 2, and 3 V. The proposed method is implemented with fixed values of $n=1$ and $V_{step}=2$ V. For simplification purposes, the first scenario considers a synthetic irradiance profile, specified in Table II, which corresponds to one repetition of the medium-to-high irradiance test described in the EN50530 dynamic test procedure [25].

TABLE II
MEDIUM-TO-HIGH IRRADIANCE TEST DESCRIBED IN EN50530 DYNAMIC TEST PROCEDURE

Slope (W/(m²·s))	Ramp up time (s)	Dwell time (s)	Ramp down time (s)	Dwell time (s)	Total duration (s)	Initial dwell time (s)	Total simulation time (s)
10	70	10	70	10	160	10	528
14	50	10	50	10	120		
20	35	10	35	10	90		
30	23	10	23	10	66		
50	14	10	14	10	48		
100	7	10	7	10	34		

Figure 10(a) represents the irradiance profile of case study 1, while Fig. 10(b) shows the irradiance ramp-rate calculated from the irradiance profile.

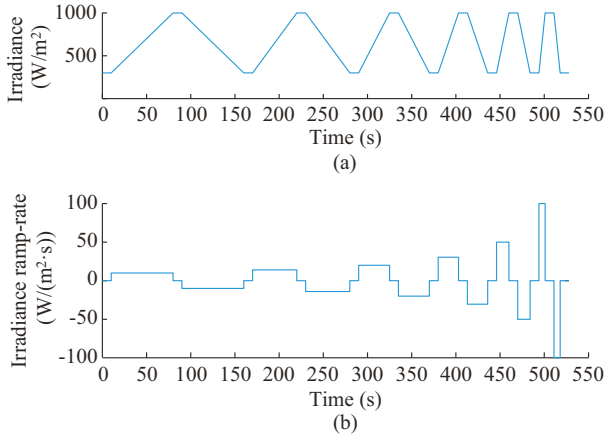

Fig. 10. Results of case study 1. (a) Irradiance profile. (b) Irradiance ramp-rate.

Figure 11 shows different power ramp-rates calculated by both methodologies with $n=1$ and varied V_{step}, namely 1, 2, and 3 V. It can be observed that the method proposed in [13] is highly dependent on the value of V_{step}. Besides, the decoupled power ramp-rate calculation method obtains a more accurate ramp-rate measurement even compared with the Sangwongwanich's case with a smaller perturbation size.

This is confirmed with the root-mean-square error (RMSE) and the mean absolute error (MAE), as calculated in (5) and (6), where r and $\hat{r}$ are the real and calculated power ramp-rates, respectively.

$$RMSE=\sqrt{\frac{1}{N}\sum_{i=1}^{N}(r(t)-\hat{r}(t))^2} \tag{5}$$

$$MAE=\frac{1}{N}\sum_{i=1}^{N}|r(t)-\hat{r}(t)| \tag{6}$$

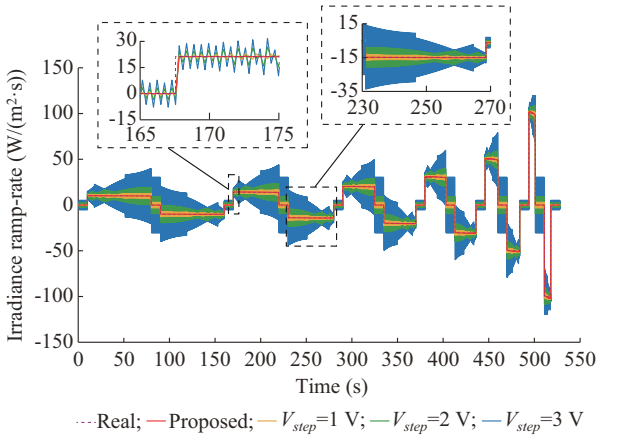

Fig. 11. Different power ramp-rates calculated by both methodologies with $n=1$ varied V_{step}.

Table III compares the RMSE and the MAE of the proposed method with the one presented in [13] with $n=1$ and varied V_{step}. In this way, it is stated that the decoupled ramp-rate calculation method allows a fast PRRC when needed by increasing the perturbation size, without affecting the computation of the power ramp-rate.

TABLE III
COMPARISON OF RMSE AND MAE OF PROPOSED METHOD AND METHOD PRESENTED IN [13] WITH $n=1$ AND VARIED V_{step}

Method	V_{step} (V)	RMSE	MAE
Method presented in [13]	1	3.5835	1.2479
	2	5.8803	4.2104
	3	14.2791	9.9060
Proposed method	2	3.2837	0.3196

A second scenario with the irradiance profile of Table II has been considered. In this scenario, the method introduced in [13] is implemented with a constant perturbation size $V_{step}=1$ V and a variable filtering value n, namely 1, 4, 5, and 10. Again, the decoupled method is configured with fixed values of $n=1$ and $V_{step}=1$ V. Figure 12 shows different irradiance ramp-rates calculated with $V_{step}=1$ V of this scenario.

As the filtering parameter is increased, the power ramp-rate measurement is filtered out. However, it is possible to observe in the zoomed part that the increased value of n produces a calculation delay proportional to n in the method presented in [13]. With the proposed method, this delay is minimized. Table IV shows the comparison of RMSE and MAE with varied n and $V_{step}=1$ V for this scenario. As can be observed, the proposed method obtains a reduced RMSE and MAE along the whole simulation.

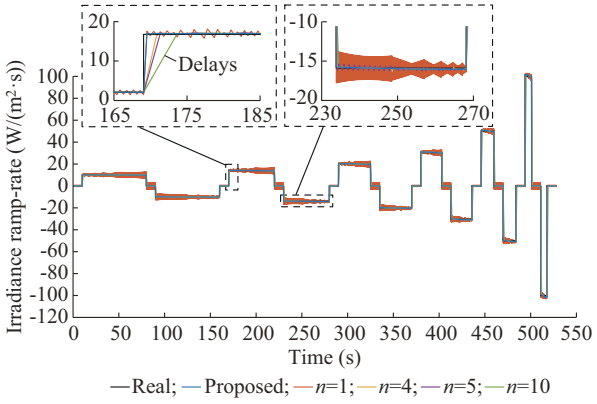

Fig. 12. Different irradiance ramp-rates calculated with $V_{step}=1$ V.

TABLE IV
COMPARISON OF RMSE AND MAE WITH VARIED n AND $V_{step}=1$ V

Method	n	RMSE	MAE
Method presented in [13]	1	3.5835	1.2479
	4	5.4989	0.7208
	5	7.3358	1.1267
	10	10.3474	1.8462
Proposed method	1	3.2795	0.3213

Figures 13 and 14 depict the evolution of RMSE and MAE along the simulation for the cases considered in Table IV, respectively. This analysis permits to identify when these methods are more accurate in relation to the size of the power ramp-rate. As can be observed, the proposed method achieves a better estimation of irradiance ramp-rate in terms of RMSE and MAE for different values of power ramp-rate.

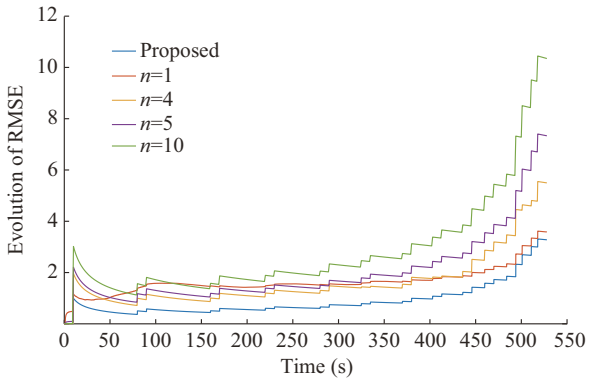

Fig. 13. Evolution of RMSE along simulation for cases considered in Table IV.

V. EXPERIMENTAL VALIDATION

The decoupled power ramp-rate calculation method has been implemented in the laboratory using hardware-in-the-loop (HIL) methodology. Two RT simulators, namely OPAL-RT 4510 and Typhoon HIL 604, have been connected in order to exchange just analogue signals. In particular, the PV plant is modelled in Typhoon HIL, while the MPPT and the power ramp-rate calculation module are allocated at OPAL-RT. In this way, Typhoon HIL sends analogue signals of PV current and voltage and OPAL-RT gives back the duty cycle signal to Typhoon HIL.

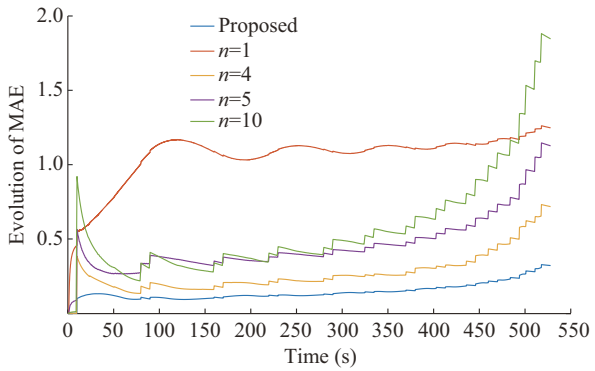

Fig. 14. Evolution of MAE along simulation for cases considered in Table IV.

This experimental validation is needed to evaluate the performance of the algorithm in the presence of noisy measurements and possible delays in the communication system. Appendix A Fig. A1 depicts the RT simulation setup.

A. Case Study 2

A scenario with a real-field irradiance profile has been test in the laboratory. The irradiance profile is the one measured by the National Resources Canada (NRCAN) datasets [26], which have high temporal resolution and make them suitable for short-term studies. In particular, a 120 s fragment of a day with a very variable cloud cover is selected, as shown in Fig. 15.

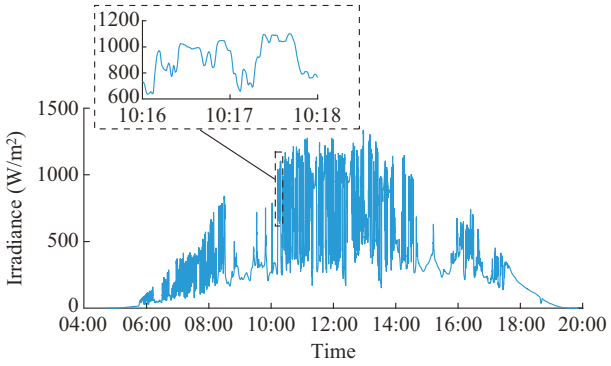

Fig. 15. Real-field highly variable irradiance profile.

The main parameters of the RT simulation are $T_M=0.5$ s and $V_{step}=4$ V. The results of case study 2 are shown in Fig. 16. As can be observed, the cases with $n=4$, $n=5$, and $n=10$ suffer from significant delays with respect to the real irradiance ramp-rate when the irradiance change is abrupt. To avoid this delay, the cases with $n=1$ follow more accurately the irradiance changes. When comparing the method presented in [13] with $n=1$ and the proposed method, it is possible to observe how the proposed method filters out the oscillations due to the MPPT algorithm.

B. Case Study 3

In the previous case studies presented in this paper, the PV system operates at the MPP. This case study emulates the PRRC condition, i.e., when the PV system is deloaded and the operation point is far from the MPP.

For this reason, when the calculated irradiance ramp-rate is greater than 10 W/(m^2·s), the reference voltage is pushed to the left of the MPP. Figure 17(a) depicts the irradiance profile used in this scenario. It consists of three consecutive trapezoidal profiles of 20, 50, and 100 W/(m^2·s). The proposed method has been implemented with $V_{step}=2$ V and two different values of T_M, namely $T_M=0.25$ s and $T_M=0.5$ s. Figure 17(b) depicts the calculated irradiance ramp-rate in the two cases with $T_M=0.25$ s and $T_M=0.5$ s. As depicted, the case with $T_M=0.5$ s obtains a softer measurement of the ramp as it is less exposed to the measurement noise errors. Figure 17(c) represents the evolution of PV voltage along with the test. It can be observed how the PV system is deloaded to the left of the MPP and that reducing T_M allows a faster PRRC.

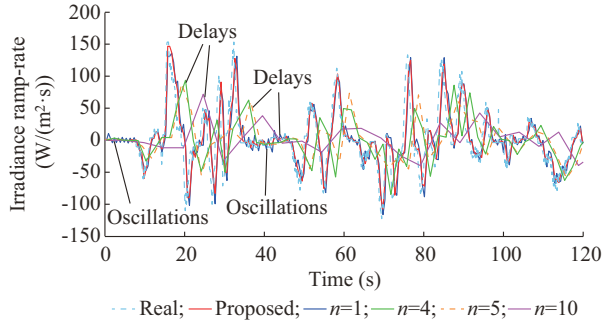

Fig. 16. Results of case study 2.

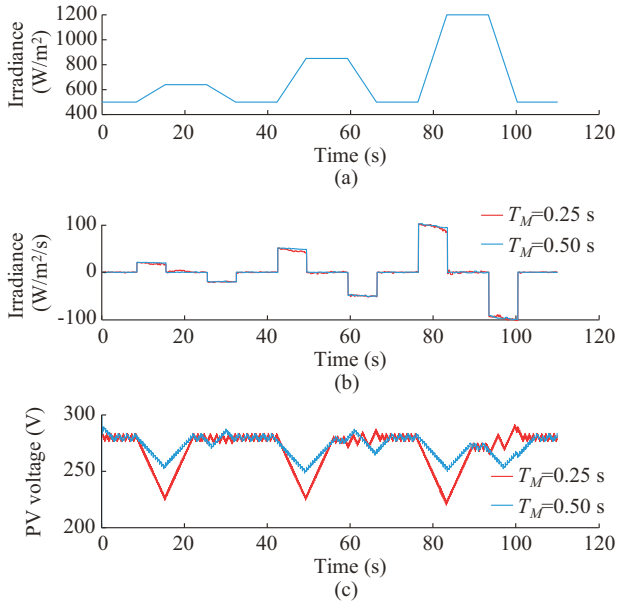

Fig. 17. Results of case study 3. (a) Irradiance profile. (b) Irradiance ramp-rate. (c) PV voltage.

VI. Conclusion

Renewable generation is required to provide advanced ancillary services for the displacement of conventional generation. One of these functionalities is the PRRC, which attempts to limit the impact of rapid fluctuations in the primary energy source. In order to develop a fast and accurate PRRC algorithm in the case of PV generators without energy storage or irradiance sensors, a method to calculate the power ramp-rate in real time is crucial. In this context, this paper proposes a novel power ramp-rate calculation method on the basis of the dP-P&O algorithm. The main advantage of this method, in contrast with previously reported ones, is that it can decouple the power ramp-rate produced by the irradiance change and the one produced by the perturbation of the MPPT algorithm. As demonstrated theoretically, this information is fundamental, as it can be used to improve the ramp-rate measurement in terms of accuracy and computation time due to its simplicity. Software simulations confirm the adequacy of the decoupled power ramp-rate calculation compared with previous methods in terms of the RMSE and MAE. Experimental results show that the proposed method is suitable for RT applications even in the worst-case scenario with a real-field highly variable irradiance profile and noisy measurements. Future studies should investigate the implementation of the proposed method in PV PRRC.

Appendix A

The RT simulation setup is given in Fig. A1 with the main elements.

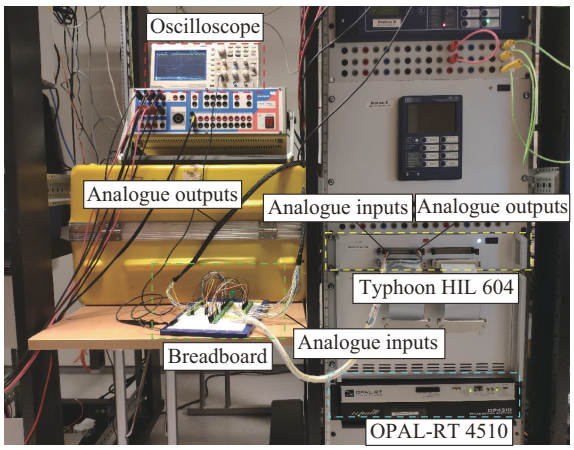

Fig. A1. RT simulation setup.

References

[1] IEA, "Trends in photovoltaic applications 2020," Tech. Rep. IEA-PVPS T1-38: 2020, International Energy Agency, Paris, France, 2020.
[2] F. M. Gonzalez-Longatt, "Impact of emulated inertia from wind power on under-frequency protection schemes of future power systems," *Journal of Modern Power Systems and Clean Energy*, vol. 4, no. 2, pp. 211-218, Mar. 2016.
[3] M. J. E. Alam, K. M. Muttaqi, and D. Sutanto, "Battery energy storage to mitigate rapid voltage/power fluctuations in power grids due to fast variations of solar/wind outputs," *IEEE Access*, vol. 9, pp. 12191-12202, Jan. 2021.
[4] A. Sangwongwanich, Y. Yang, and F. Blaabjerg, "Development of flexible active power control strategies for grid-connected photovoltaic inverters by modifying MPPT algorithms," in *Proceedings of the IFEEC and ECCE Asia*, Kaohsiung, China, Jun. 2017, pp. 87-92.
[5] V. Gevorgian and S. Booth, "Review of PREPA technical requirements for interconnecting wind and solar generation," Tech. Rep. NREL/TP-5D00-57089, National Renewable Energy Laboratory, Golden, USA, 2013.
[6] A. Hoke, "Smart inverter utility experience in Hawaii," in *Proceedings of IEEE PES General Meeting Tutorial on Smart Inverters for Distributed Generators*, Atlanta, USA, Aug. 2019, pp. 1-27.
[7] A. Nelson, A. Nagarajan, K. Prabakar *et al.*, "Hawaiian electric advanced inverter grid support function laboratory validation and analy-

sis," Tech. Rep. NREL/TP-5D00-67485, National Renewable Energy Laboratory, Golden, USA, 2016.
[8] X. Chen, Y. Du, H. Wen *et al.*, "Forecasting-based power ramp-rate control strategies for utility-scale PV systems," *IEEE Transactions on Industrial Electronics*, vol. 66, no. 3, pp. 1862-1871, Mar. 2019.
[9] L. Yao, B. Yang, H. Cui *et al.*, "Challenges and progresses of energy storage technology and its application in power systems," *Journal of Modern Power Systems and Clean Energy*, vol. 4, no. 4, pp. 519-528, Jul. 2016.
[10] S. Sukumar, M. Marsadek, K. R. Agileswari *et al.*, "Ramp-rate control smoothing methods to control output power fluctuations from solar photovoltaic (PV) sources–a review," *Journal of Energy Storage*, vol. 20, pp. 218-229, Apr. 2018.
[11] H. Xin, Y. Liu, Z. Wang *et al.*, "A new frequency regulation strategy for photovoltaic systems without energy storage," *IEEE Transactions on Sustainable Energy*, vol. 4, no. 4, pp. 985-993, Oct. 2013.
[12] W. A. Omran, M. Kazerani, S. Member *et al*., "Investigation of methods for reduction of power fluctuations generated from large grid-connected photovoltaic systems," *IEEE Transactions on Energy Conversion*, vol. 26, no. 1, pp. 318-327, Mar. 2011.
[13] A. Sangwongwanich, Y. Yang, and F. Blaabjerg, "A cost-effective power ramp-rate control strategy for single-phase two-stage grid-connected photovoltaic systems," in *Proceedings of 2016 IEEE Energy Conversion Congress and Exposition (ECCE)*, Milwaukee, USA, Sept. 2016, pp. 1-7.
[14] N. Femia, G. Petrone, G. Spagnuolo *et al.*, "Optimization of perturb and observe maximum power point tracking method," *IEEE Transactions on Power Electronics*, vol. 20, no. 4, pp. 963-973, Jul. 2005.
[15] A. Pandey, N. Dasgupta, and A. K. Mukerjee, "High-performance algorithms for drift avoidance and fast tracking in solar MPPT system," *IEEE Transactions on Energy Conversion*, vol. 23, no. 2, pp. 681-689, Jul. 2008.
[16] X. Li, H. Wen, B. Chen *et al.*, "A cost-effective power ramp rate control strategy based on flexible power point tracking for photovoltaic system," *Solar Energy*, vol. 208, pp. 1058-1067, Sept. 2020.
[17] D. Sera, R. Teodorescu, J. Hantschel *et al.*, "Optimized maximum power point tracker for fast-changing environmental conditions," *IEEE Transations on Industrial Electronics*, vol. 55, no. 7, pp. 2629-2637, Jul. 2008.
[18] X. Li, Q. Wang, H. Wen *et al.*, "Comprehensive studies on operational principles for maximum power point tracking in photovoltaic systems," *IEEE Access*, vol. 7, pp. 121407-121420, Aug. 2019.
[19] J. S. Ko, J. H. Huh, and J. C. Kim, "Overview of maximum power point tracking methods for PV system in micro grid," *Electronics*, vol. 9, no. 5, pp. 1-22, May 2020.
[20] M. Y. Javed, A. F. Mirza, A. Hasan *et al.*, "A comprehensive review on a PV based system to harvest maximum power," *Electronics*, vol. 8, no. 12, p. 1480, Dec. 2019.
[21] J. M. Riquelme-Dominguez and S. Martinez, "Comparison of different photovoltaic perturb and observe algorithms for drift avoidance in fluctuating irradiance conditions," in *Proceedings of 2020 IEEE International Conference on Environment and Electrical Engineering and 2020 IEEE Industrial and Commercial Power Systems Europe (EEEIC/I&CPS Europe)*, Madrid, Spain, Jun. 2020, pp. 1-5.
[22] B. Mohandes, M. S. El Moursi, N. Hatziargyriou *et al.*, "A review of power system flexibility with high penetration of renewables," *IEEE Transactions on Power Systems*, vol. 34, no. 4, pp. 3140-3155, Jul. 2019.
[23] M. J. Alam, K. M. Muttaqi, and D. Sutanto, "A novel approach for ramp-rate control of solar PV using energy storage to mitigate output fluctuations caused by cloud passing," *IEEE Transactions on Energy Conversion*, vol. 29, no. 2, pp. 507-518, Jun. 2014.
[24] The MathWorks Inc. (2019, Dec.). MATLAB and Electrical Simscape Toolbox. [Online]. Available: https://www. mathworks. com/products/simscape-electrical.html
[25] *Overall Efficiency of Grid Connected Photovoltaic Inverters*, CENELEC standard EN50530, 2010.
[26] Natural Resources Canada (NRCAN). (2020, Feb.). High resolution solar radiation datasets. [Online]. Available: https://www.nrcan.gc.ca/energy/renewable-electricity/solar-photovoltaic/18409

Jose Miguel Riquelme-Dominguez received the electrical engineering degree from the Universidad de Sevilla, Seville, Spain, in 2015. His employment experience included the Spanish Transmission System Operator, and Red Electrica de Espana. Since 2018, he has been with the Department of Electrical Engineering, Universidad Politecnica de Madrid, Madrid, Spain, where he is currently a Ph.D. student and Assistant Professor. His research interests include grid connected photovoltaic systems and power system stability and control.

Francisco M. Gonzalez-Longatt is currently a full Professor of electrical power engineering with the Department of Electrical Engineering, Information Technology and Cybernetics, University of South-Eastern Norway. He is the author or editor of several books (Spanish and English). He is a Member of IET and CIGRE. He received the Professional Recognition as the Fellow of the Higher Education Academy (FHEA), in January 2014. He is the Vicepresident of the Venezuelan Wind Energy Association. He is also an Associate Editor in several journals with an impressive track record in scientific publications. His research interest includes innovative (operation/control) schemes to optimize the performance of future energy systems.

Sergio Martinez received the M.Sc. degree in industrial engineering, and the Ph.D. degree in electrical engineering from Universidad Politecnica de Madrid, Madrid, Spain, in 1993 and 2001, respectively. He is an Associate Professor with the Department of Electrical Engineering, Escuela Tecnica Superior de Ingenieros Industriales, Universidad Politecnica de Madrid. His research interests include electrical generation from renewable energy and the provision of ancillary services from electrical equipment connected to power systems through power electronics.